IVYSPRING INTERNATIONAL PUBLISHER

Theranostics

2012; 2(1):76-85. doi: 10.7150/thno.3462

Research Paper

Comparison of Two Ultrasmall Superparamagnetic Iron Oxides on Cytotoxicity and MR Imaging of Tumors

Mulan Li[1,3,†], Hoe Suk Kim[1,2,†], Lianji Tian[1,3], Mi Kyung Yu[4], Sangyong Jon[4], Woo Kyung Moon[1,2,3] ✉

1. Department of Radiology, Seoul National University Hospital, 101 Daehangno, Jongno-gu, Seoul 110-744, Korea
2. The Institute of Radiation Medicine, Medical Research Center, Seoul National University, 101 Daehangno, Jongno-gu, Seoul 110-744, Korea
3. Department of Biomedical Science, College of Medicine, Seoul National University, Seoul, 101 Daehangno, Jongno-gu, Seoul 110-744, Korea
4. Cell Dynamics Research Center, School of Life Sciences, Gwangju Institute of Science and Technology, 261 Chemdangwagi-ro, Gwangju 500–712, Korea

† These authors contributed equally to this work.

✉ Corresponding author: WK Moon, Department of Radiology, Seoul National University Hospital, 101 Daehangno, Jongno-gu, Seoul 110-744, Republic of Korea. Tel: 82-2-2072-3928, E-mail: moonwk@snu.ac.kr

Received: 2011.08.30; Accepted: 2011.11.04; Published: 2012.01.01

Abstract

Purpose: This study was performed to compare the cytotoxicity and magnetic resonance (MR) contrast in diverse cultured cells and xenograft tumors models of two ultra-small superparamagnetic iron oxides (USPIOs), thermally cross-linked superparamagnetic iron oxide nanoparticles (TCL-SPION) and monocrystalline iron oxide nanoparticles (MION-47).

Materials and methods: Transmission electron microscopy (TEM) images and R_2 relaxivity values of the TCL-SPION and MION-47 were obtained and the cell viability and cell growth velocity of treated and untreated human fibroblasts and human umbilical vein endothelial cells (HUVEC) were evaluated. The effect of TCL-SPION and MION-47 on the secretion of interlukin-6 (IL-6) and tumor necrosis factor-alpha (TNF-α), the production of nitric oxides and the mitochondrial membrane potentials in murine macrophage cells (RAW264.7) was compared. Human hepatocellular carcinoma cells (HepG2, $5x10^5$) were subcutaneously injected into nude mice (BALB/c) and *in vivo* MR imaging of tumors before and after injection with TCL-SPION or MION-47 (12.5 mg Fe/kg) was performed on a 1.5 Tesla MRI scanner.

Results: On TEM images, the average core diameter of TCL-SPION was 9 nm whereas that of MION-47 was 5 nm. TCL- SPION (345.0 ± 6.2 $mM^{-1}sec^{-1}$) had higher relaxivity (R_2) than MION-47 (130.7 ± 1.1 $mM^{-1}sec^{-1}$). Significant changes in cell viability and growth were not found in human fibroblasts and HUVEC exposed to TCL-SPION and MION-47. However, IL-6 and TNF-α secretions increased dose-dependently and significantly in the macrophages treated with MION-47 or TCL-SPION. TCL-SPION had a lower stimulatory effect on IL-6 secretions than did MION-47 (P <0.05) and nitric oxides were produced in the macrophages by MION-47 but not TCL-SPION. A change in the mitochondrial membrane potential of the macrophages was observed 24 hours after the exposure, and MION-47 induced more collapses of the mitochondrial membrane potential than did TCL-SPION. In the *in vivo* MR imaging, 33.0 ± 1.3% and 7.5 ± 0.4% signal intensity decrease on T_2*-weighted images was observed in the tumors injected with TCL-SPION and MION-47, respectively.

Conclusion: Due to the modified surface properties and larger core size of its iron oxide nanoparticles, TCL-SPION achieves lower cytotoxicity and better tumor MR contrast than

MION-47. Our study suggests that TCL-SPION may be used as a new platform for tumor imaging and therapy monitoring.

Key words: Ultra-small superparamagnetic iron oxides, Magnetic resonance imaging, TCL-SPION, MION-47, Tumor targeting.

Introduction

Ultra-small superparamagnetic iron oxide (USPIO, <50 nm) is appears to be suitable for the single particle platform to assess targeting imaging and therapy *in vivo* [1-3]. Monocrystalline iron oxide nanoparticle (MION-47, 20−25 nm overall diameter) is a commercially available [4] and has been widely used to assess functional MR imaging [5], vascular imaging [6], and measurement of macrophage activity in a number of diseases [7]. However, tumor targeting effect of MION-47 is limited and serious side effects of these USPIO have been reported in clinical trials for evaluation of nodal metastases in known cancer patients [8-10]. Recently our group developed a novel USPO, thermal cross-linked superparamagnetic iron oxide nanoparticle (TCL-SPION, 20−30 nm overall diameter) which is synthesized by a simple thermal cross-linking method using Si-OH-containing copolymer [11]. TCL-SPION has been applied as multi-functional nanoparticle for metastatic tumors imaging in lymph nodes [12], for targeted cancer therapy by conjugation with cancer-specific ligands and anti-cancer drugs [13, 14], for *in vivo* bimodal imaging by combination with optical probes [11] and for genes delivery [15].

In contrast to the prototype dextran coating of MION-47 [8], the surface of TCL-SPION was specifically modified with the protein- or cell-resistant polymer, poly(TMSMA-*r*-PEGMA-*r*-NAS) [16]. The surface modification of nanoparticles provides mainly the benefits of protection from rapid degradation and aggregation, reduction in toxicity and improved the enhanced permeability and retention (EPR) effect for tumor targeting *in vivo* [17-20]. Furthermore, the adjusting surface coating thickness and materials can affect the magnetic property of nanoparticles [21]. The diverse cytotoxic properties of these nanoparticles by the modification of surface coating have been reported. For example, the accumulated nanoparticles diminished the cell proliferation and viability resulting from cytoskeletal changes and reactive oxygen species (ROS) production [22, 23]. The degraded nanoparticles also affected cellular function and homeostasis [24-28].

Various nanoparticles are under development as molecular imaging agents for the detection of tumors and treatment monitoring. In prior to biomedical application of novel nanoparticles, however, the toxicological effect and the biodistribution of nanoparticles should be carefully evaluated. In present study, we evaluated the magnetic properties, the cytotoxicity and the tumor imaging efficiency of a novel iron oxide nanoparticle, TCL-SPION compared with MION-47 as a reference. TCL-SPION exhibited higher relaxivity (R_2 value), lower cytotoxicity in cultured cells and more intense MR contrast effects in tumor imaging than did MION-47.

Materials and Methods

USPIOs and *in vitro* MR imaging

The TCL-SPION was obtained from the Gwangju Institute of Science and Technology (GIST). The MION-47 was purchased from CMIR, Massachusetts General Hospital of Harvard University. The *in vitro* MR imaging of the phantoms associated with varying concentrations of nanoparticles was performed using a 3 Tesla clinical MR scanner (Siemens Healthcare, Erlangen, Germany). For measurements of the R_2 values, a multiple spin-echo sequence with a repetition time (TR) of 5000 ms and a viable echo time (TE, 16, 32, 48, 64 ms) was used. The common acquisition parameters were as follows: field of view (FOV) = 147 × 157 mm, and matrix size = 320 × 300.

Cell culture

Human fibroblasts isolated from dermis and peripheral blood monocytes were cultured in Dulbecco's modified Eagle medium (WelGENE, Daegu, Korea) supplemented with 10% FBS (WelGENE) and a 1% antibiotic solution containing penicillin and streptomycin. Human umbilical vein endothelial cells (HUVEC) were cultured in an endothelial cell growth medium EGM-2 MV BulletKit (Lonza, Verviers, Belgium) on a gelatin-coated culture dish. RAW264.7 mouse macrophage cells and Hep G2 human liver cancer cells were cultured in RPMI 1640 (WelGENE) with 10% FBS and 1% penicillin and streptomycin. All the cells were cultured in a 5% CO_2 incubator at 37°C.

Cell viability and growth

To evaluate the cytotoxicity of TCL-SPION and MION-47, human fibroblasts, HUVEC and RAW264.7 cells were incubated in medium containing

TCL-SPION or MION-47 (10, 25, 50, 100, 250, 500, 1000 μg Fe/mL) for 24 hours, and cell viability was assessed by flow cytometry analysis using 7-AAD (BD PharmingenTM, Franklin Lakes, NJ, USA). The cell-associated fluorescence was measured using a FACSCalibur flow cytometer (BD Biosciences). The data were analyzed with the CellQuest v3.3 software (BD Biosciences).

To evaluate the influence of TCL-SPION and MION-47 on cell growth, human fibroblasts and HUVEC were seeded in 6-well tissue culture plates at 1×10^4 cells/well and were further cultured after adding 100 μg Fe/mL of TCL-SPION or MION-47. The number of cells cultured with or without USPIO was counted on days 1, 2 and 3 using a hemocytometer.

Cytokines secretion and nitric oxide production in macrophage

An enzyme-linked immunospecific assay (ELISA) was performed to evaluate whether USPIO elicits the production of the proinflammatory cytokines in macrophages. In brief, RAW264.7 cells were seeded in a 24-well tissue culture plate at 5×10^4 cells/well. After treatment with TCL-SPION or MION-47 at concentrations of 25 μg Fe/mL and 50 μg Fe/mL for 24 hours, the levels of interleukin-6 (IL-6) or tumor necrotic factor-alpha (TNF-α) secreted by RAW264.7 were measured using an enzyme-linked immunosorbent assay kit (R&D, Minneapolis, MN, USA).

To investigate the effect of USPIO on nitric oxide production in mouse macrophages, nitrite was assayed by the Griess reaction [27]. Briefly, the culture supernatants from the RAW264.7 cells treated with TCL-SPION or MION-47 at concentrations of 25 μg Fe/mL, 50 μg Fe/mL and 100 μg Fe/mL for 24 hours were collected, and 100 μl of the Griess reagent (0.5% sulfanilamide, 0.05% N-(1-Naphthyl) ethylenediamine and 2.5% phosphoric acid) was added to 100 μl of the supernatant in a 96-well plate. The absorbance was measured at 540 nm using a microplate reader, and the nitrite concentration was calculated from a standard sodium nitrite curve.

Mitochondrial membrane potential

To evaluate the changes in the mitochondrial membrane potential of macrophage cells treated with TCL-SPION or MION-47, the fluorescence of JC-1 (Molecular Probes, Eugene, OR, USA), which fluoresces differently in healthy cells with the intact mitochondria and apoptotic cells in which the mitochondrial membrane potential has collapsed, was analyzed. In healthy cells, JC-1 is taken up by the mitochondria, where it forms aggregates exhibiting intense red fluorescence. In cells with depolarized mitochondria potential, JC-1 remains in the cytoplasm, where it fluoresces green.

In brief, after treatment with TCL-SPION or MION-47 at concentrations of 50 μg Fe/mL for 24 hours, RAW264.7 cells were incubated in a buffer containing 2 μM of JC-1 for 15–20 minutes at 37℃. The JC-1 stained cells were suspended in the culture media and immediately analyzed using flow cytometry or fluorescence microscopy. The images of the cells were acquired with a fluorescence microscope (Leica, Wetzlar, Germany) equipped with a CCD camera (Leica). The cell fluorescence was concomitantly assessed with a FACSCalibur flow cytometer (BD Biosciences).

Measurement of total cellular iron levels

The cellular iron levels were measured using the Total Iron Reagent Set (Pointe Scientific, Canton, MI, USA). Briefly, the cells were incubated in medium supplemented with USPIO (0, 50, 100, 200 μg Fe/mL) for 24 hours. After washing with PBS twice, the cells were enumerated. The collected cells were resuspended in 6 N HCl and incubated at 70°C for 30 minutes. The total iron levels were measured according to the manufacturer's instructions, and the average cellular iron concentration was calculated by dividing the total mean values by the number of cells.

In vivo MR imaging

To develop the tumor model, approximately 6-week old BALB/c-nude mice were anesthetized, and 5×10^5 Hep G2 cells suspended in 0.1 mL matrigel (BD Biosciences) were subcutaneously injected into the back right flank.

When the tumor reached 5-8 mm diameter as measured with a digital caliper, *in vivo* MR imaging studies were performed using a 1.5T clinical MR scanner (Sigma Horizon; GE Medical Systems, Milwaukee, WI) with a human wrist coil after tail vein injection of 5, 12.5, 30 mg Fe/kg of USPIOs. The MR images of the tumors were obtained before and at 4 and 24 hours after the intravenous injection using gradient echo sequence (TR = 12.5 ms, TE = 5.9 ms, FOV = 70 × 70, flip angle = 15°, matrix = 256 × 256, NEX = 2.0 and section thickness = 2 mm) and 3D FIESTA-COR pulse sequence (TR=7.7 ms, TE = 3.2 ms, FOV = 80 × 80, flip angle = 45°, matrix = 190 × 190, NEX = 2.0 and section thickness = 2 mm).

To determine the signal intensity (SI) changes in the MR images of the tumors, regions of interest (ROIs) were drawn along the margin of each tumor and the left thigh muscle on representative T_2*-

weighted MR images. The ratio of SI changes for tumor versus muscle was calculated according to the formula:

$$SI\ ratio = [SI_{tumor\ (post\text{-}USPIO)} / SI_{muscle\ (post\text{-}USPIO)}] / [SI_{tumor\ (pre\text{-}USPIO)} / SI_{muscle\ (pre\text{-}USPIO)}]$$

Prussian blue staining and immunostaining

To examine the intracellular distributions of TCL-SPION and MION-47, the TCL-SPION and MION-47 treated cells were fixed in 4% paraformaldehyde and stained with Prussian blue. Briefly, the fixed cells were washed 3 times with PBS, incubated for 30 minutes with 5% potassium ferrocyanide (Sigma, St. Louis, MO, USA) in 5% hydrochloric acid, rewashed and counterstained with nuclear fast red (Sigma) for 20 minutes.

After the MR imaging was completed, the tumor-bearing mice were sacrificed and the tumors were carefully removed. The tumors were fixed in 10% formalin, embedded in regular paraffin wax and cut into 4 μm sections. The paraffin sections were dewaxed and hydrated. The presence of TCL-SPION or MION-47 in tumor sections was detected by Prussian blue staining. Macrophages were detected using antibodies for CD 68 (Santacruz, Santa Cruz, CA, USA). After incubation with the appropriate secondary antibody, the sections were stained with diaminobenzidine solution (Dako, Hamburg, Germany) for 2–5 minutes.

Statistical analysis

Means ± standard errors were calculated from at least three independent experiments and statistically evaluated using a one-way ANOVA model followed by the Student-Newman-Keuls test. For all tests, *p*-values less than 0.05 were considered statistically significant.

Results

Comparison of the magnetic properties of TCL-SPION and MION-47

The schematics of TCL-SPION and MION-47 and physicochemical parameters are shown in Figure 1A.

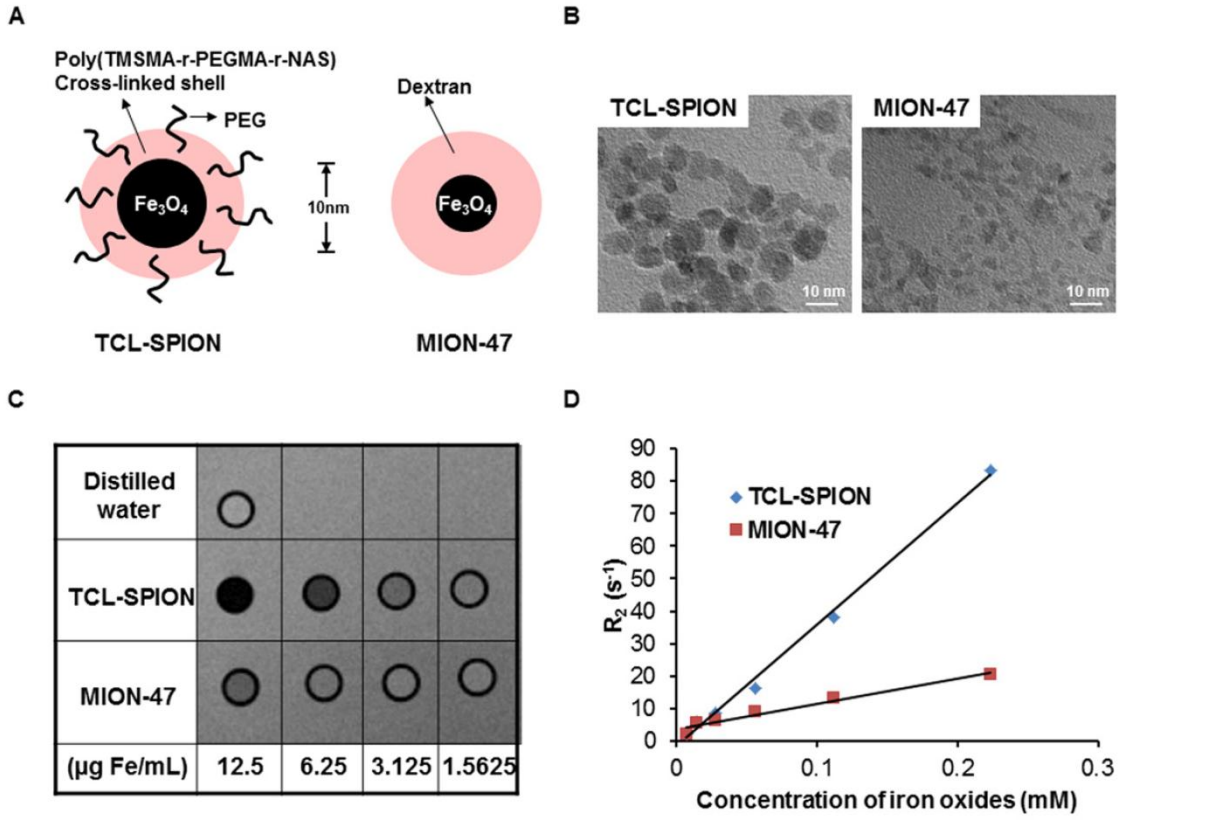

Figure 1. Physicochemical parameters and comparison of magnetic properties. (A) A schematic representation of TCL-SPION and MION-47. (B) TEM image of TCL-SPION and MION-47. (C) A T_2-weighted MR image of TCL-SPION and MION-47 at various iron oxide concentrations. At identical iron oxide concentrations, TCL-SPION had a more intense MR contrast effect than MION-47. (D) Plots of the R_2 ($1/T_2$) value. The relaxivity (R_2) of TCL-SPION (345.0 ± 6.2 $mM^{-1}sec^{-1}$, blue) was higher than that of MION-47 (130.7 ± 1.1 $mM^{-1}sec^{-1}$, red).

From transmission electron microscopy (TEM) images, the average core diameter of TCL-SPION was 9 nm, whereas that of MION-47 was 5 nm. The relaxivities ($1/T_2=R_2$) of TCL-SPION and MION-47 dispersed in distilled water were measured using a 3 Tesla MR scanner. The R_2 of TCL-SPION and MION-47 were 345.0 ± 6.2 $mM^{-1}sec^{-1}$ and 130.7 ± 1.1 $mM^{-1}sec^{-1}$, respectively. At identical iron concentrations, TCL-SPION showed the more intense MR contrast effect compared to MION-47 (Fig. 1B).

In vitro evaluation of cytotoxicity in human normal cells

To compare the cellular toxicities of TCL-SPION and MION-47, we first evaluated cell viability in normal human cells (human fibroblasts and HUVEC). A reduction in human fibroblasts and HUVEC viability was not observed after 24 hours of exposure to increasing concentrations of TCL-SPION and MION-47 (up to 1 mg Fe/mL) (Fig. 2A, B). TCL-SPION and MION-47 (up to 1 mg Fe/mL) were not taken up by the human fibroblasts and HUVEC (Supplementary Material: data 1). When human fibroblasts and HUVEC were exposed to 100 μg Fe/mL of TCL-SPION or MION-47 separately for 3 days, there was no effect on the cell growth velocity (Fig. 2C, D).

In vitro evaluation of cytokines release and nitric oxide production in macrophages

We compared the influences of TCL-SPION and MION-47 on proinflammatory cytokine release in mouse macrophage cells. The RAW264.7 cells phagocytized the TCL-SPION and MION-47 within 2 hours. There was no significant difference in the accumulation of two USPIOs in the RAW264.7 cells until 24 hours (Supplementary Material: data 2, $P > 0.05$). The IL-6 and TNF-α releases in the RAW264.7 cells were dose-dependently and significantly increased by adding TCL-SPION and MION-47 (Fig. 3A, B, $P < 0.001$). MION-47 showed a greater stimulatory effect on IL-6 release than did TCL-SPION (Fig. 3A). TCL-SPION and MION-47 showed similar stimulatory effects on TNF-α (Fig. 3B).

The effect of TCL-SPION and MION-47 on nitric oxide production in macrophages was also evaluated. MION-47 induced a dose-dependent and significant increase in nitric oxide production (Fig. 3C, $P < 0.001$). However, TCL-SPION did not have any stimulatory effects on nitric oxide production in the RAW264.7 cells (Fig. 3C).

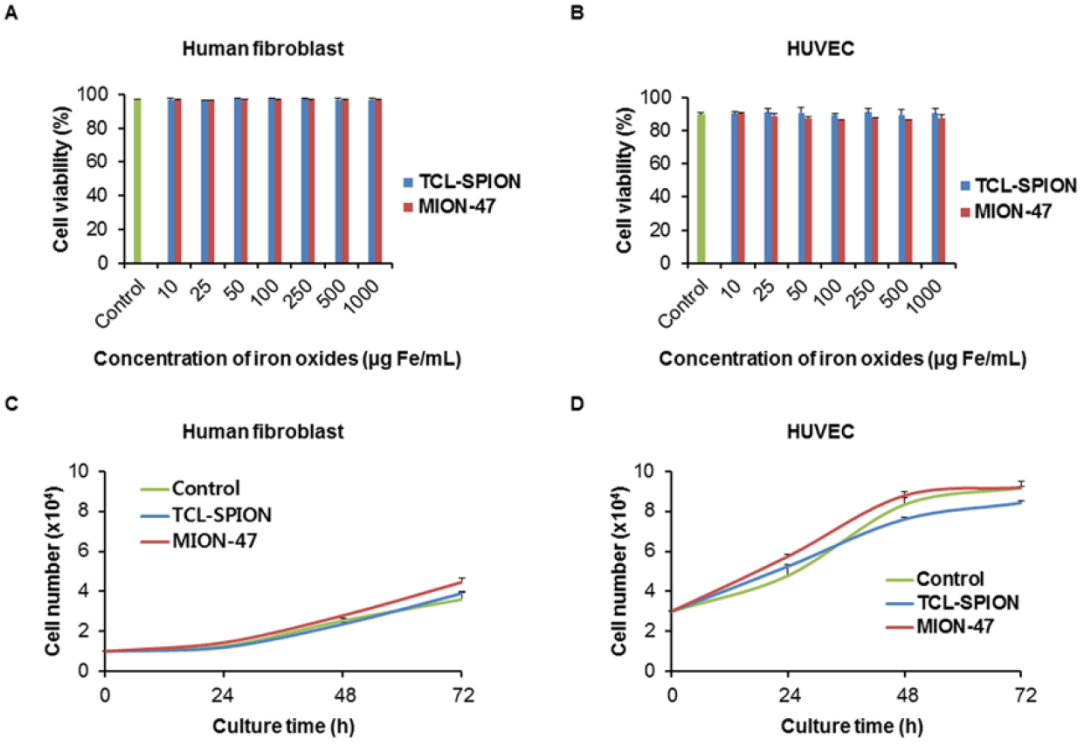

Figure 2. *In vitro* evaluation of cytotoxicity in human normal cells. (A, B) The viabilities of human fibroblasts and human umbilical vein endothelial cells (HUVEC) were assessed by MTT assay. A reduction in the viability of human fibroblasts and HUVEC was not observed after 24 hours of exposure to increasing concentrations of TCL-SPION and MION-47 (up to 1 mg Fe/mL). (C, D) The growth velocity was assessed by a trypan blue assay. The human fibroblasts and HUVEC were exposed to 100 μg Fe/mL of TCL-SPION or MION-47 separately for 3 days, and there was no effect on the cell growth velocity. The data are presented as the means ± standard errors from at least three independent experiments.

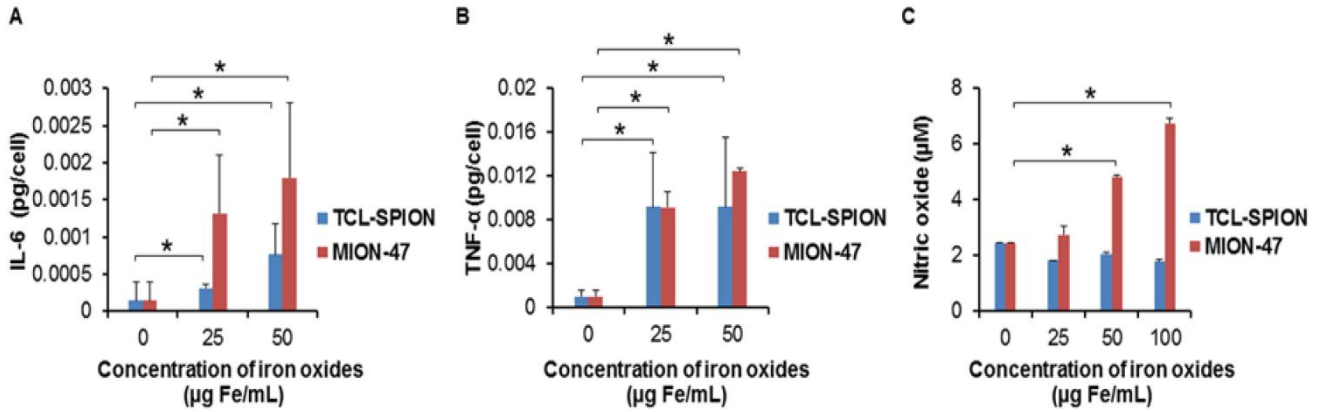

Figure 3. ***In vitro*** **evaluation of cytokines release and nitric oxide production in macrophage.** The levels of (A) IL-6 and (B) TNF-α released from mouse macrophage cells (RAW264.7). RAW264.7 cells were treated with TCL-SPION or MION-47 at concentrations of 25 μg Fe/mL and 50 μg Fe/mL for 24 hours. The IL-6 and TNF-α releases in the RAW264.7 cells were dose-dependently and significantly increased by adding TCL-SPION and MION-47 (*, $P < 0.001$, vs. control). MION-47 showed a greater stimulatory effect on IL-6 release than did TCL-SPION, while the TNF-α stimulatory effect was similar. (C) Nitric oxide production in macrophages. Macrophages were treated TCL-SPION or MION-47 at concentrations of 25 μg Fe/mL, 50 μg Fe/mL and 100 μg Fe/mL for 24 hours. The nitrite levels were assayed by the Griess reaction. MION-47 induced a dose-dependent and significant increase in nitric oxide production (*, $P < 0.001$, vs. control), but TCL-SPION did not have any stimulatory effect on nitric oxide production. All data are presented as the means ± standard errors from at least three independent experiments.

Mitochondrial membrane potential of macrophage

The iron oxide-mediated stress impact on macrophage cells was determined by evaluating the changes in mitochondrial membrane potentials using JC-1. Flow cytometry analysis revealed that treatment with TCL-SPION or MION-47 gradually reduced the population of healthy cells (red fluorescence in the JC-1 assay, Fig. 4A) and caused a collapse of the mitochondrial membrane potential (green fluorescence in the JC-1 assay) in a small population of RAW264.7 cells after 24 hours (Fig. 4B). The H_2O_2 treatment (500 μM) resulted in a collapse of the mitochondria membrane potential in most cells within 2 hours (Fig. 4B). When comparing the influences of TCL-SPION and MION-47 on the mitochondrial membrane, the MION-47-treated cells emitted more green fluorescence than did those treated with TCL-SPION, implying that MION-47 is more cytotoxic than TCL-SPION (Fig. 4B).

In vivo MR imaging

For *in vivo* biodistribution study, we injected two USIPOs into the tail veins of the normal mice and the decrease in MR signal intensity was found in the liver and spleen. There was no signal drop in the heart, kidney and brain (Supplementary Material: data 3). When we compared the different concentration of TCL-SPION and MION-47 for tumor imaging, MR images with 12.5 mg Fe/kg showed best tumor contrast. The tumors in subcutaneous layers appeared as hyperintense areas in T_2*-weighted MR images before the injections (Fig. 5A). At 4 hours post-injection, noticeable darkening appeared in the tumor areas, indicating an accumulation of TCL-SPION within the tumor (Fig. 5A). The changes in signal intensity were calculated in the ROIs of the T_2*-weighted images. The tumor signal intensity of the mice injected with TCL-SPION decreased by 33.0 ± 1.3%, and this lower signal intensity was maintained at 24 hours post-injection (Fig. 5B, $P < 0.01$). However, no significant changes in post-injection signal intensity (7.5 ± 0.4%) were observed in the MION-47 group (Fig. 5B).

We tested whether Hep G2 cells take up TCL-SPION and MION-47 after 24 hours of incubation in concentrations of 10, 100 and 500 μg Fe/mL. No uptake of TCL-SPION or MION-47 into the Hep G2 was detected (Supplementary Material: data 2A).

Histological examination

In normal mice, TCL-SPION and MION-47 were taken up by phagocytic cells of the liver and spleen, such as Kuffer cells, macrophages and monocytes whereas there were no accumulation of USPIO in the brain, heart and kidney tissue (Supplementary Material: data 3).

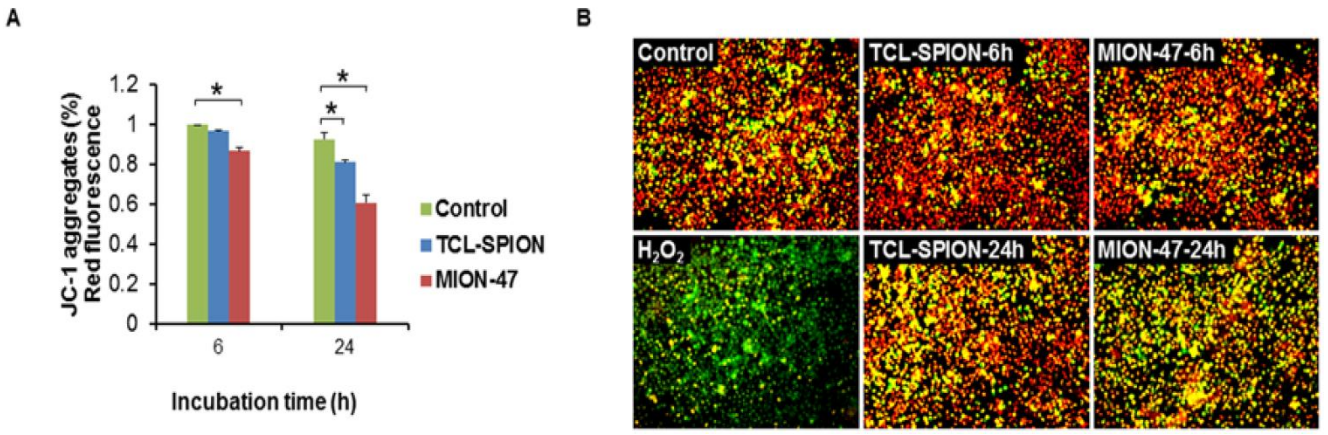

Figure 4. **Mitochondrial membrane potential of macrophage.** (A) Flow cytometry analysis of JC-1 in macrophages. Macrophages were treated with TCL-SPION or MION-47 at a concentration of 50 μg Fe/mL for 6 hours and 24 hours. The TCL-SPION and MION-47 treatments gradually reduced the population of healthy cells (the JC-1 aggregates). (*, $P < 0.05$, vs. control) (B) Fluorescence image of JC-1 aggregates (red) and JC-1 monomers (green) in macrophages. The MION-47 treated cells emitted more green fluorescence than did the TCL-SPION treated cells. All data are presented as the means ± standard errors from at least three independent experiments.

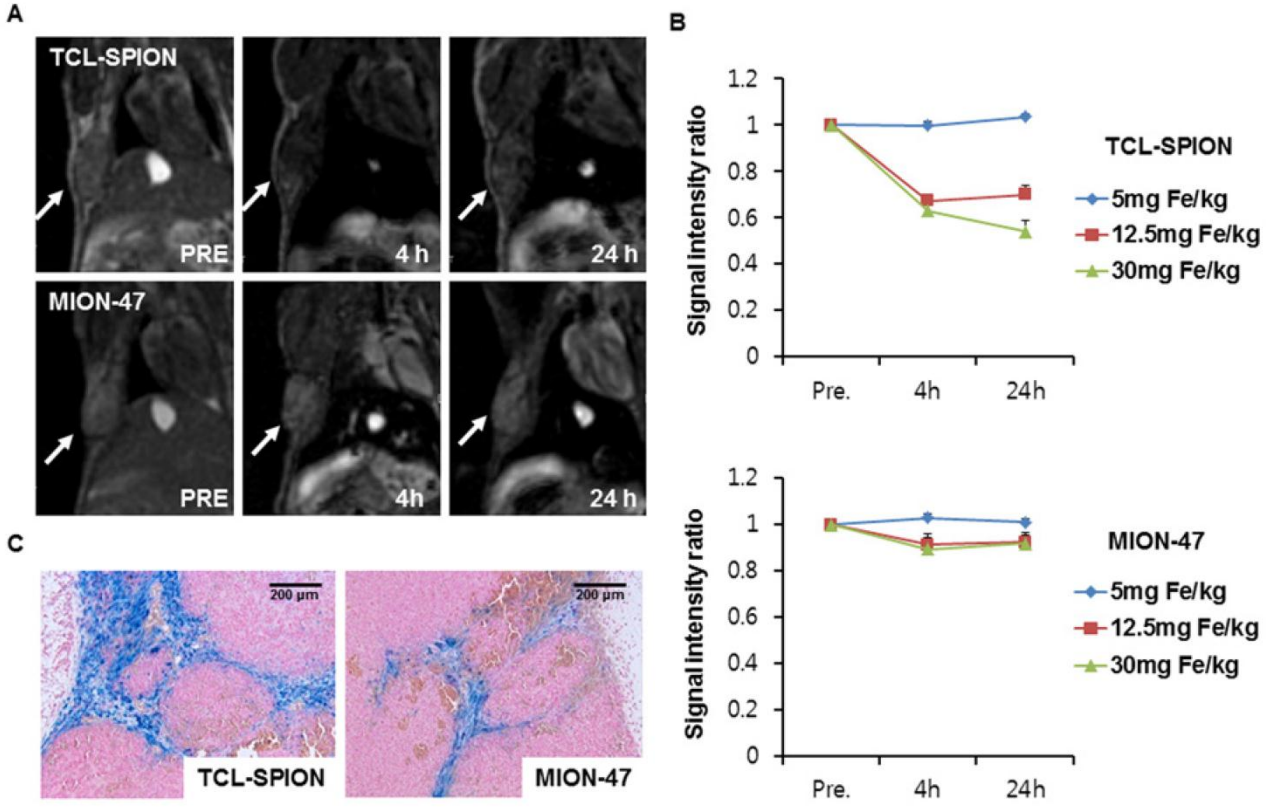

Figure 5. ***In vivo* MR imaging.** (A) T_2*-weighted images of tumor-bearing mice injected with 12.5 mg Fe/kg of TCL-SPION or MION-47. After injection with TCL-SPION, a noticeable darkening appeared in the tumor area, indicating a large accumulation of TCL-SPION within the tumor. In the mice injected with MION-47, there was no considerable difference in the pre-injection and post-injection tumor signal intensities. (B) The changes in signal intensity measured on T_2*-weighted tumor images. The tumor signal intensity of the mice injected with TCL-SPION was decreased by 33.0 ± 1.3%. MION-47 did not cause a significant change in signal intensity after injection (7.5 ± 0.4%). (C) Prussian blue staining of tumor microsections. More TCL-SPION was accumulated in the tumors than MION-47. All data are presented as the means ± standard errors from at least three independent experiments.

Prussian blue staining of tumor sections was performed to examine the distribution of TCL-SPION and MION-47 in the tumors. There was greater accumulation of TCL-SPION than MION-47 in the tumors (Fig. 5C). To further investigate the precise location of the accumulated TCL-SPION and MION-47 in the tumors, we performed Prussian blue staining and CD 68 immunostaining in center and periphery of tumor section. Immunohistological analysis showed that TCL-SPION and MION-47 were accumulated in center areas of tumors but not periphery of the tumors, where large numbers of macrophages were found (Data not shown). The greater accumulation of TCL-SPION than MION-47 was observed around the tumor blood vessels.

Discussion

Magnetic relaxivity of iron oxide nanoparticles is mainly determined by iron core size, composition, and crystalline phase. As compared mass magnetization values with various-size magnetism-engineered iron oxide nanoparticles, it was demonstrated the smaller the nanoparticles, the weaker their net magnetic moment because of the large contribution of canted magnetic spin states on the surface [29]. Furthermore, recent paper suggested that the coating thickness and material of iron oxide nanoparticles can affected the R_2 values [21]. Among these physicochemical parameters, the big differences between MION-47 and TCL-SPION are iron core size and surface coating. On TEM images, the average core diameter of TCL-SPION was 9 nm whereas that of MION-47 was 5 nm. In contrast to the prototype dextran coating of MION-47 [8, 30], the surface of TCL-SPION was specifically modified with the protein- or cell-resistant polymer, poly(TMSMA-*r*-PEGMA-*r*-NAS) [16]. In our study, the TCL-SPION (R_2 = 345.0 ± 6.2 $mM^{-1}S^{-1}$) showed much higher relaxivity than that of the MION-47 (R_2 = 130.7 ± 1.1 $mM^{-1}S^{-1}$), which were mainly determined by the large iron core sizes and might be affected by the different surface modification.

Biocompatibility and minimal biofouling properties are the requirements that an MR contrast agent must meet to be successfully used in MR imaging *in vivo*. Therefore, it is necessary to engineer the surfaces of nanoparticles to minimize biofouling and aggregation under harsh physiological conditions (i.e., high salt and protein concentrations) [16, 31]. Consistent with previous reports [32, 33], there was no uptake of TCL-SPION or MION-47 by normal human cells, even at high concentrations, and hence no long-term cytotoxicity in normal human cells. Substantial amount of USPIO was taken by liver and spleen macrophages after intravenous injection [34]. Upon ingestion of toxic substances, macrophages may release cytokines, such as TNF-α and IL-6, to induce further inflammatory or immune responses [35]. In the present study, both TCL-SPION and MION-47 exposure stimulated the production TNF-α and IL-6 by macrophages. There was greater stimulation of TNF-α release by MION-47. When we investigated macrophage toxicity by a nitric oxide production assay, TCL-SPION did not stimulate nitric oxide production, while MION-47 increased nitric oxide production remarkably. Nitric oxide is a highly reactive free radical and the role of nitric oxide in macrophage toxicity is well established [36]. In the present study, the toxic effect of TCL-SPION and MION-47 on the mitochondrial function of macrophages was evaluated. MION-47 induced more collapses of the mitochondrial membrane potential than did TCL-SPION. This result indicates that MION-47 is more cytotoxic and can induce more macrophage cell death than TCL-SPION.

The EPR effect allows small nanoparticles to permeate the large fenestrations present in abnormal blood vessels of tumor [4, 37]. As a tumor-targeting strategy, the EPR effect of nanoparticles is a key mechanism for solid tumor targeting. The EPR effect is tunable by modifying the surface, charge or size of the nanoparticles or by manipulating the tumor microenvironment [38, 39]. Modification of the nanoparticle surface is important for improving the EPR effect as well as reducing the agglomeration of nanoparticles and proteins in body fluids. The TCL-SPION including multiple "protein-repelling" PEG groups in the cross-linked polymer coating layers indicated relatively high protein resistance than dextran-coated nanoparticles in the serum-containing physiological medium [14]. Although MION-47 is similar to TCL-SPION in size, their hydrophilic dextran coat may be susceptible to blood protein adsorption, thus reducing the dispersal of MION-47. In this study, TCL-SPION was more accumulated than MION-47 in the tumors and most USPIOs were observed around the tumor blood vessels. Our study demonstrated that TCL-SPION was more effective in tumor targeting because of increased accumulation and high relaxivity of TCL-SPION as compared with MION-47.

In conclusion, TCL-SPION exhibited lower *in vitro* cytotoxicity and better tumor MR contrast than MION-47. Our study suggests that TCL-SPION may be used as a new platform for *in vivo* tumor imaging and therapy monitoring.

Supplementary Material

Supplementary data 1: Prussian blue staining of human fibroblast and human umbilical vein endothelial cell

(HUVEC) incubated with TCL-SPION and MION-47. Supplementary data 2: Analysis of iron oxide uptake in cancer cells and macrophage incubated with TCL-SPION and MION-47. Supplementary data 3: *In vivo* biodistribution of TCL-SPION and MION-47.
http://www.thno.org/v02p0076s1.pdf

Acknowledgements

This study was supported by a grant from the National R & D Program for Cancer Control, Ministry of Health & Welfare (A01185), by a grant from the Innovative Research Institute for Cell Therapy, Republic of Korea (Grant no. A062260), by the National Research Foundation of Korea (NRF) grant funded by the Korea government (MEST) (2011–0000174, 2011–0005381, 2011–0003657 and 2011–0004322), and by the second stage of Brain Korea 21 (BK21) program in 2011. M. Lee and L. Tian were recipients of fellowships from the BK21 programs.

Conflict of Interest

The authors have declared that no conflict of interest exists.

References

1. Benderbous S, Corot C, Jacobs P, Bonnemain B. Superparamagnetic agents: physicochemical characteristics and preclinical imaging evaluation. Acad Radiol. 1996;3 Suppl 2:S292-4.
2. Huang P, Li Z, Lin J, Yang D, Gao G, Xu C, Bao L, Zhang CL, Wang K, Song H, Hu HY, Cui DX. Photosensitizer-conjugated magnetic nanoparticles for in vivo simultaneous magnetofluorescent imaging and targeting therapy. Biomaterials. 2011;32:3447-58.
3. Wunderbaldinger P, Josephson L, Weissleder R. Crosslinked iron oxides (CLIO): a new platform for the development of targeted MR contrast agents. Acad Radiol. 2002;9 Suppl 2:S304-6.
4. Moghimi SM, Hunter AC, Murray JC. Nanomedicine: current status and future prospects. FASEB J. 2005;19:311-30.
5. Leite FP TD, Vanduffel W, Fize D, Sasaki Y, Wald LL, Dale AM, Kwong KK, Orban GA, Rosen BR, Tootell RB, Mandeville JB. Repeated fMRI using iron oxide contrast agent in awake, behaving macaques at 3 Tesla. Neuroimage. 2002;16:283-294.
6. Bremer C, Mustafa M, Bogdanov A, Jr., Ntziachristos V, Petrovsky A, Weissleder R. Steady-state blood volume measurements in experimental tumors with different angiogenic burdens a study in mice. Radiology. 2003;226:214-20.
7. Denis MC, Mahmood U, Benoist C, Mathis D, Weissleder R. Imaging inflammation of the pancreatic islets in type 1 diabetes. Proc Natl Acad Sci U S A. 2004;101:12634-9.
8. Shen T, Weissleder R, Papisov M, Bogdanov A, Jr., Brady TJ. Monocrystalline iron oxide nanocompounds (MION): physicochemical properties. Magn Reson Med. 1993;29:599-604.
9. Choi SH, Moon WK. Contrast-enhanced MR imaging of lymph nodes in cancer patients. Korean J Radiol. 2010;11:383-94.
10. Choi SH, Han MH, Moon WK, Son KR, Won JK, Kim JH, et al. Cervical lymph node metastases: MR imaging of gadofluorine M and monocrystalline iron oxide nanoparticle-47 in a rabbit model of head and neck cancer. Radiology. 2006;241:753-62.
11. Lee H, Yu MK, Park S, Moon S, Min JJ, Jeong YY, Kang HW, Jon S. Thermally cross-linked superparamagnetic iron oxide nanoparticles: synthesis and application as a dual imaging probe for cancer in vivo. J Am Chem Soc 2007;129:12739-45.
12. Lim SW, Kim HW, Jun HY, Park SH, Yoon KH, Kim HS, Jon S, Yu MK, Juhng SK. TCL-SPION-enhanced MRI for the detection of lymph node metastasis in murine experimental model. Acad Radiol. 2011;18:504-11.
13. Yu MK, Park J, Jeong YY, Moon WK, Jon S. Integrin-targeting thermally cross-linked superparamagnetic iron oxide nanoparticles for combined cancer imaging and drug delivery. Nanotechnology. 2010;21:415102.
14. Yu MK, Kim D, Lee IH, So JS, Jeong YY, Jon S. Image-guided prostate cancer therapy using aptamer-functionalized thermally cross-linked superparamagnetic iron oxide nanoparticles. Small. 2011;7:2241-9.
15. Namgung R, Singha K, Yu MK, Jon S, Kim YS, Ahn Y, Park IK, Kim WJ. Hybrid superparamagnetic iron oxide nanoparticle-branched polyethylenimine magnetoplexes for gene transfection of vascular endothelial cells. Biomaterials 2010;31:4204-13.
16. Lee H, Lee E, Kim do K, Jang NK, Jeong YY, Jon S. Antibiofouling polymer-coated superparamagnetic iron oxide nanoparticles as potential magnetic resonance contrast agents for in vivo cancer imaging. J Am Chem Soc. 2006;128:7383-9.
17. Wang YX, Hussain SM, Krestin GP. Superparamagnetic iron oxide contrast agents: physicochemical characteristics and applications in MR imaging. Eur Radiol. 2001;11:2319-31.
18. Ruan J, Wang K, Song H, Xu X, Ji J, Cui D. Biocompatibility of hydrophilic silica-coated CdTe quantum dots and magnetic nanoparticles. Nanoscale Res Lett. 2011;6:299.
19. Corot C, Robert P, Idee JM, Port M. Recent advances in iron oxide nanocrystal technology for medical imaging. Adv Drug Deliv Rev. 2006;58:1471-504.
20. Peer D KJ, Hong S, Farokhzad OC, Margalit R, Langer R. . Nanocarriers as an emerging platform for cancer therapy. Nat Nanotechnol. 2007;2:751-760.
21. LaConte LE, Nitin N, Zurkiya O, Caruntu D, O'Connor CJ, Hu X, Bao G. Coating thickness of magnetic iron oxide nanoparticles affects R2 relaxivity. J Magn Reson Imaging. 2007;26:1634-41.
22. Soenen SJ, Himmelreich U, Nuytten N, Pisanic TR, 2nd, Ferrari A, De Cuyper M. Intracellular nanoparticle coating stability determines nanoparticle diagnostics efficacy and cell functionality. Small. 2010;6:2136-45.
23. Soenen SJ, Nuytten N, De Meyer SF, De Smedt SC, De Cuyper M. High intracellular iron oxide nanoparticle concentrations affect cellular cytoskeleton and focal adhesion kinase-mediated signaling. Small. 2010;6:832-42.
24. Apopa PL, Qian Y, Shao R, Guo NL, Schwegler-Berry D, Pacurari M, Porter D, Shi X, Vallyathan V, Castranova V, Flynn DC. Iron oxide nanoparticles induce human microvascular endothelial cell permeability through reactive oxygen species production and microtubule remodeling. Part Fibre Toxicol. 2009;6:1.
25. Keenan CR, Goth-Goldstein R, Lucas D, Sedlak DL. Oxidative stress induced by zero-valent iron nanoparticles and Fe(II) in human bronchial epithelial cells. Environ Sci Technol. 2009;43:4555-60.
26. Lunov O, Syrovets T, Buchele B, Jiang X, Rocker C, Tron K, Nienhaus GU, Walther P, Mailänder V, Landfester K, Simmet T. The effect of carboxydextran-coated superparamagnetic iron oxide nanoparticles on c-Jun N-terminal kinase-mediated apoptosis in human macrophages. Biomaterials. 2010;31:5063-71.
27. Kim HS, Choi Y, Song IC, Moon WK. Magnetic resonance imaging and biological properties of pancreatic islets labeled with iron oxide nanoparticles. NMR Biomed. 2009;22:852-6.

28. Kim HS, Oh SY, Joo HJ, Son KR, Song IC, Moon WK. The effects of clinically used MRI contrast agents on the biological properties of human mesenchymal stem cells. NMR Biomed. 2010;23:514-22.
29. Jun YW, Huh YM, Choi JS, Lee JH, Song HT, Kim S, Yoon S, Kim KS, Shin JS, Suh JS, Cheon J. Nanoscale size effect of magnetic nanocrystals and their utilization for cancer diagnosis via magnetic resonance imaging. J Am Chem Soc. 2005;127:5732-3.
30. Wong KA, et al. In Vitro Relaxivities Studies of Gadolinium Carbon Nanotubes at 3T. Proc Intl Soc Mag Reson Med. 2008; 16:1665.
31. Gupta AK, Gupta M. Synthesis and surface engineering of iron oxide nanoparticles for biomedical applications. Biomaterials. 2005;26:3995-4021.
32. Sun R, Dittrich J, Le-Huu M, Mueller MM, Bedke J, Kartenbeck J, Lehmann WD, Krueger R, Bock M, Huss R, Seliger C, Gröne HJ, Misselwitz B, Semmler W, Kiessling F. Physical and biological characterization of superparamagnetic iron oxide- and ultrasmall superparamagnetic iron oxide-labeled cells: a comparison. Invest Radiol. 2005;40:504-13.
33. Jayapaul J, Hodenius M, Arns S, Lederle W, Lammers T, Comba P, Kiessling F, Gaetjens J. FMN-coated fluorescent iron oxide nanoparticles for RCP-mediated targeting and labeling of metabolically active cancer and endothelial cells. Biomaterials. 2011;32:5863-71.
34. Briley-Saebo KC, Johansson LO, Hustvedt SO, Haldorsen AG, Bjornerud A, Fayad ZA, Ahlstrom HK. Clearance of iron oxide particles in rat liver: effect of hydrated particle size and coating material on liver metabolism. Invest Radiol. 2006;41:560-71.
35. Pestka S LJ, Zoon KC, Samuel CE. Interferons and their actions. Annu Rev Biochem. 1987;56:727-777.
36. Lakics V, Vogel SN. Lipopolysaccharide and ceramide use divergent signaling pathways to induce cell death in murine macrophages. J Immunol. 1998;161:2490-500.
37. Maeda H. The enhanced permeability and retention (EPR) effect in tumor vasculature: the key role of tumor-selective macromolecular drug targeting. Adv Enzyme Regul. 2001;41:189-207.
38. Gambarota G, van Laarhoven HW, Philippens M, Peeters WJ, Rijken P, van der Kogel A, Punt CJ, Heerschap A. Assessment of Blood Hemodynamics by USPIO-Induced R(1) Changes in MRI of Murine Colon Carcinoma. Appl Magn Reson. 2010;38:349-360.
39. Hyodo F, Chandramouli GV, Matsumoto S, Matsumoto K, Mitchell JB, Krishna MC, Munasinghe JP. Estimation of tumor microvessel density by MRI using a blood pool contrast agent. Int J Oncol. 2009;35:797-804.